Figure F16. Biostratigraphic summary chart of Site 1122 showing correlation between the four microfossil biohorizons and age assignments. Numbers are ages (Ma).

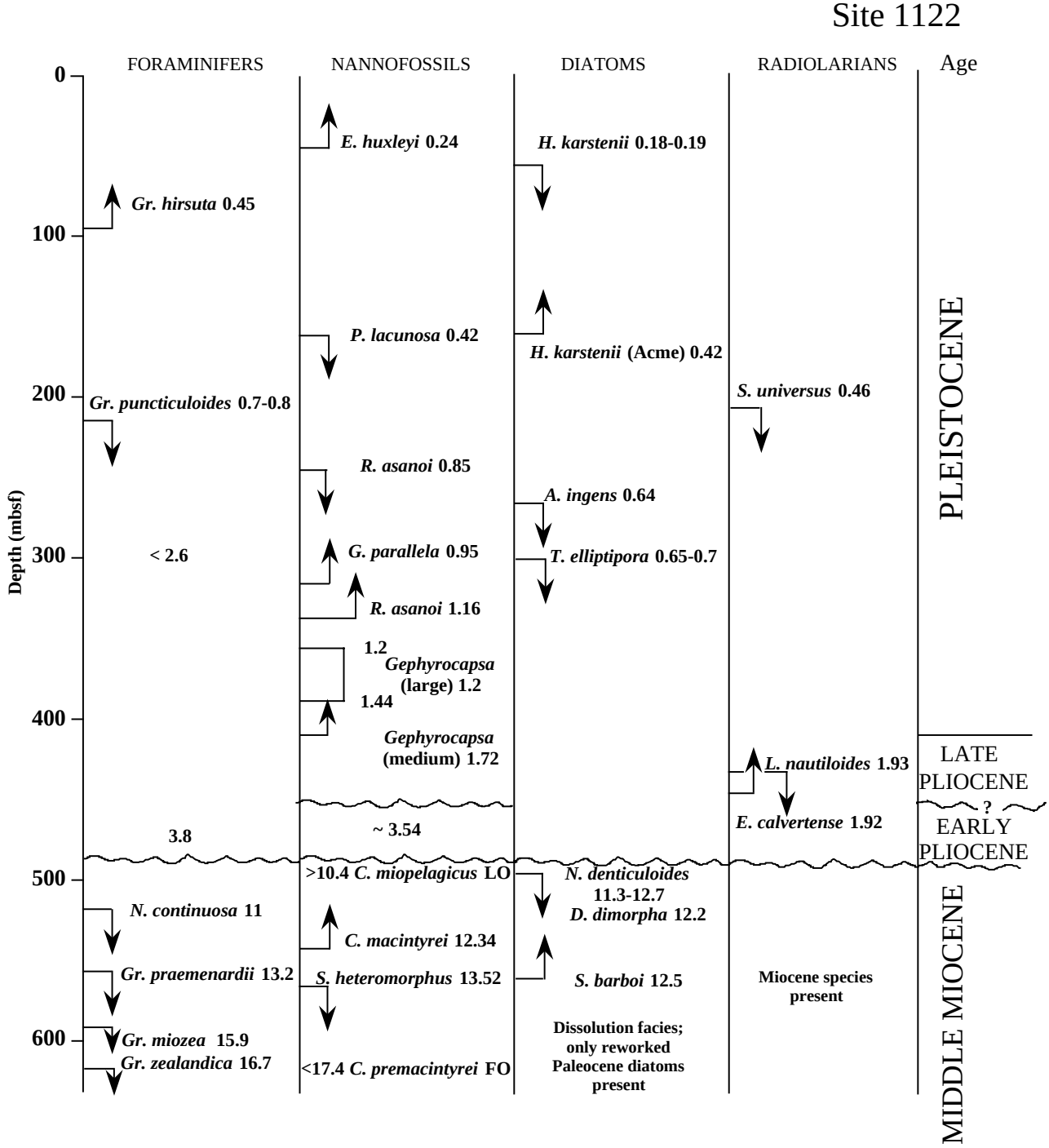

Figure F17. Age-depth curve using multiple microfossil and polarity chron datums for Hole 1122C. The best fit line is drawn according to subjective weighting of the chronostratigraphic and geochronologic precision of the events and approximate average rate of sedimentation. Numbers by datums (e.g., F1) denote events listed in Table T8, p. 127. Wavy line at 490 mbsf represents a stratigraphic disconformity.

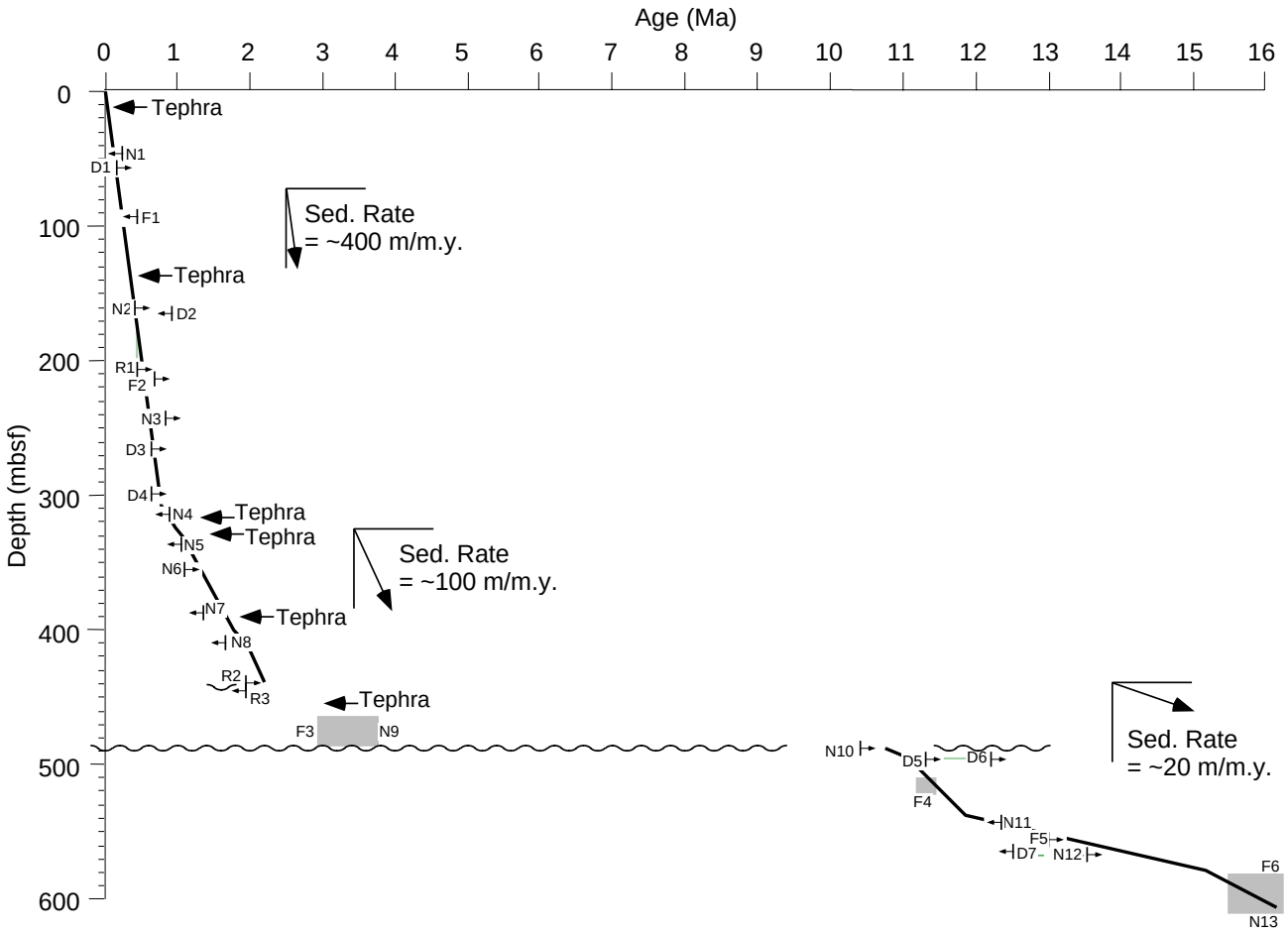

Figure F18. Summary of the changing characteristics of the foraminiferal faunas at Site 1122.

Litho-stratigraphic Unit		Planktonic Fauna	Benthic Fauna		
UNIT I A B C	Turbidite-dominated	Normal, well-preserved, oceanic fauna	Deep-water assemblage with addition of small shelf and bathyal forms		Pliocene-Pleistocene
UNIT I D	Turbidite-dominated	Normal, well-preserved, oceanic fauna	Only deep-water assemblage		Pliocene-Pleistocene
UNIT II A	Contourite-dominated	Large, thick-walled, oceanic fauna, few or no small forms	Only deep-water assemblage	Dissolution	Pliocene-Pleistocene
UNIT II B	Contourite-dominated	Barren or rapidly buried fauna of small forms (winnowings) - minor reworked Oligocene	Barren or only deep-water assemblage	Dissolution	Miocene
UNIT III A	Debris flows and coarse sediments	Variable oceanic fauna	Only deep-water assemblage	Dissolution	Miocene
UNIT III B	Debris flows and coarse sediments	Normal oceanic fauna	Dominantly mid-shelf fauna (large and small) with minor deep-water assemblage		Miocene

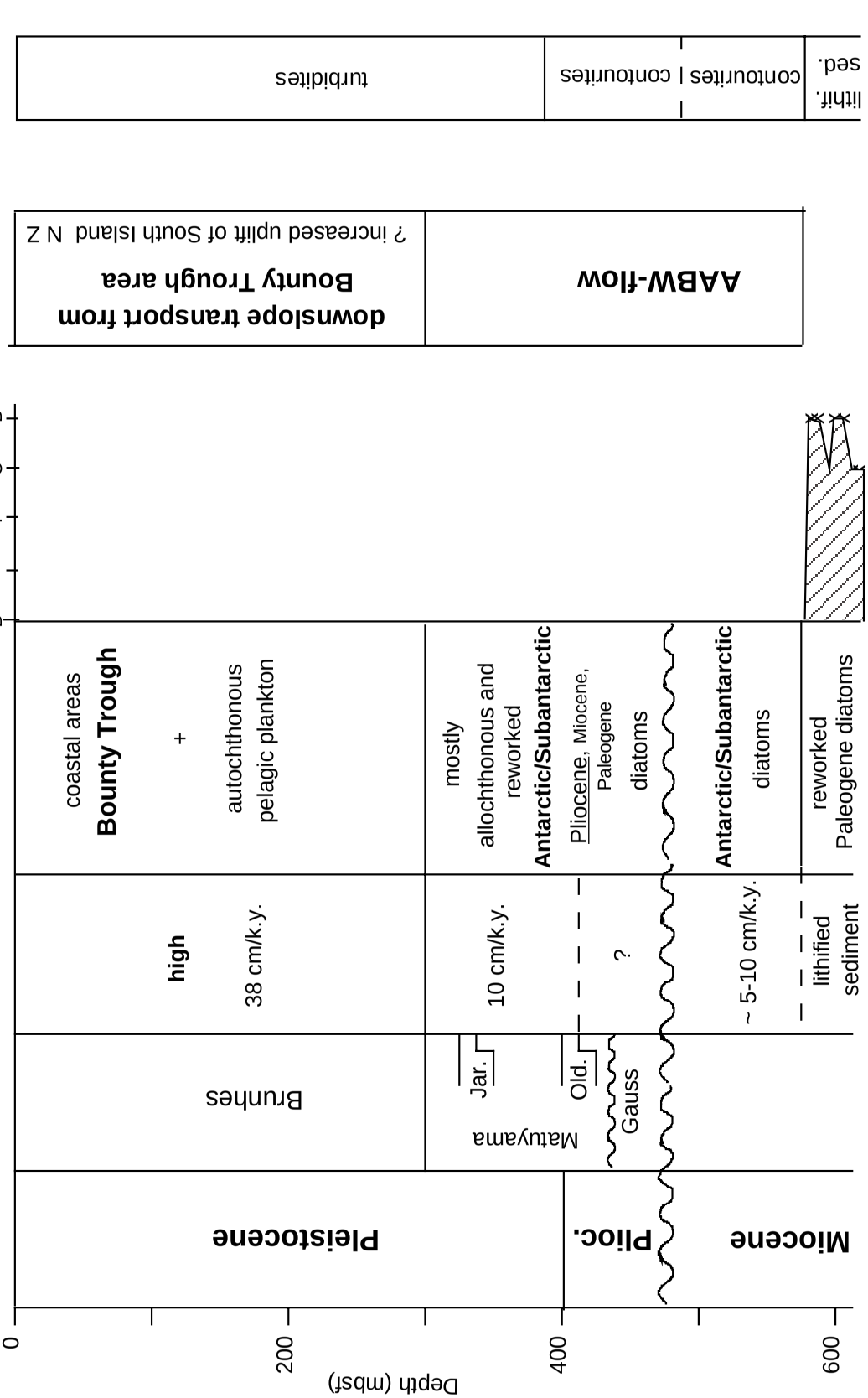

Figure F19. Provenance of diatoms in the Neogene of Hole 1122C and implications for a major change in processes responsible for major sediment input.

Figure F20. Whole-core magnetic susceptibility from Hole 1122C from the Bartington loop of the shipboard automated multisensor track, archive-half continuous measurements of NRM intensity, and intensity of remanence after 20 mT of demagnetization from the pass-though cryogenic magnetometer. Vertical and subvertical lines in the lower 500 mbsf of the hole indicate intervals of nonrecovery of core.

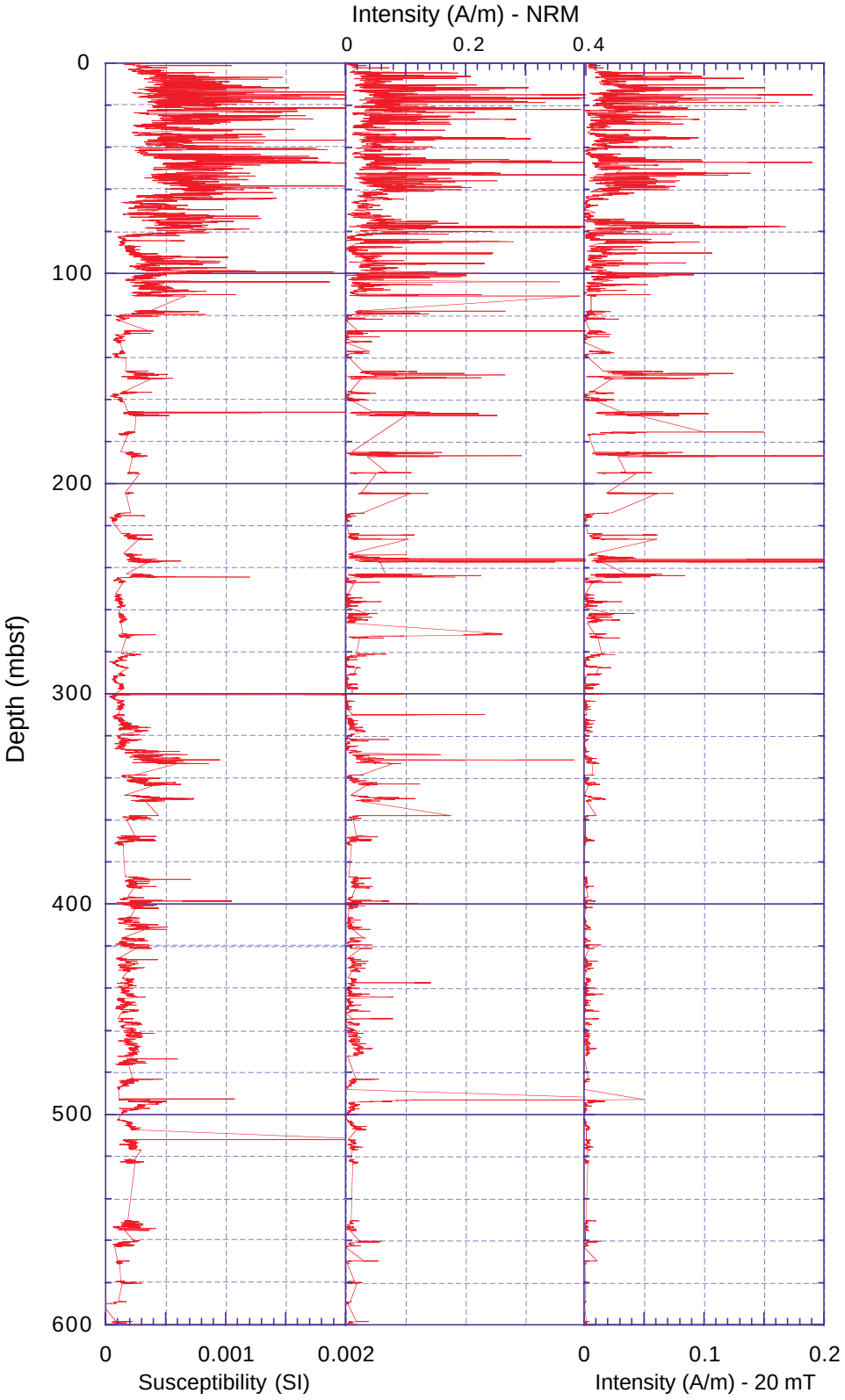

Figure F21. Whole-core inclination of Hole 1122C after alternating-field demagnetization to 20 mT on the pass-though cryogenic magnetometer. Polarity interpretation is given on the right. Black (white) shaded intervals indicate normal (reversed) polarity and hatched shading indicates intervals where polarity could not be determined because of poor recovery. Chrons are identified from correlation with the GPTS (Cande and Kent, 1995; Berggren et al., 1995) constrained by biostratigraphy (see discussion in **"Biostratigraphy,"** p. 13, and Fig. **F25,** p. 66).

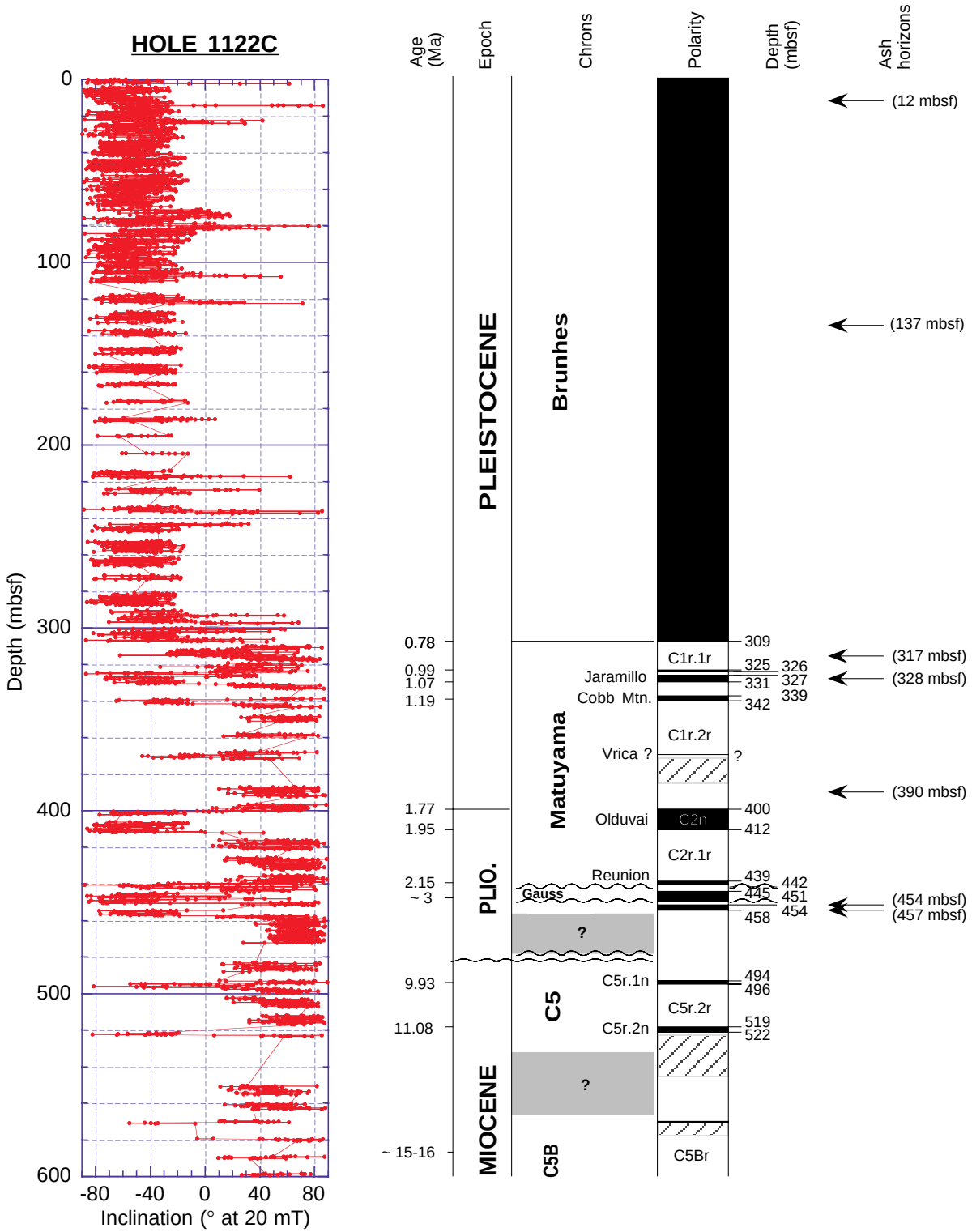

Figure F22. A–I. Vector component diagrams of AF demagnetization behavior of representative discrete samples from Hole 1122C. A, B, G, I show a reversed field drilling-induced overprint on normal polarity samples. B, C show radial remagnetization from attempts to demagnetize samples with AF fields above 50 mT.

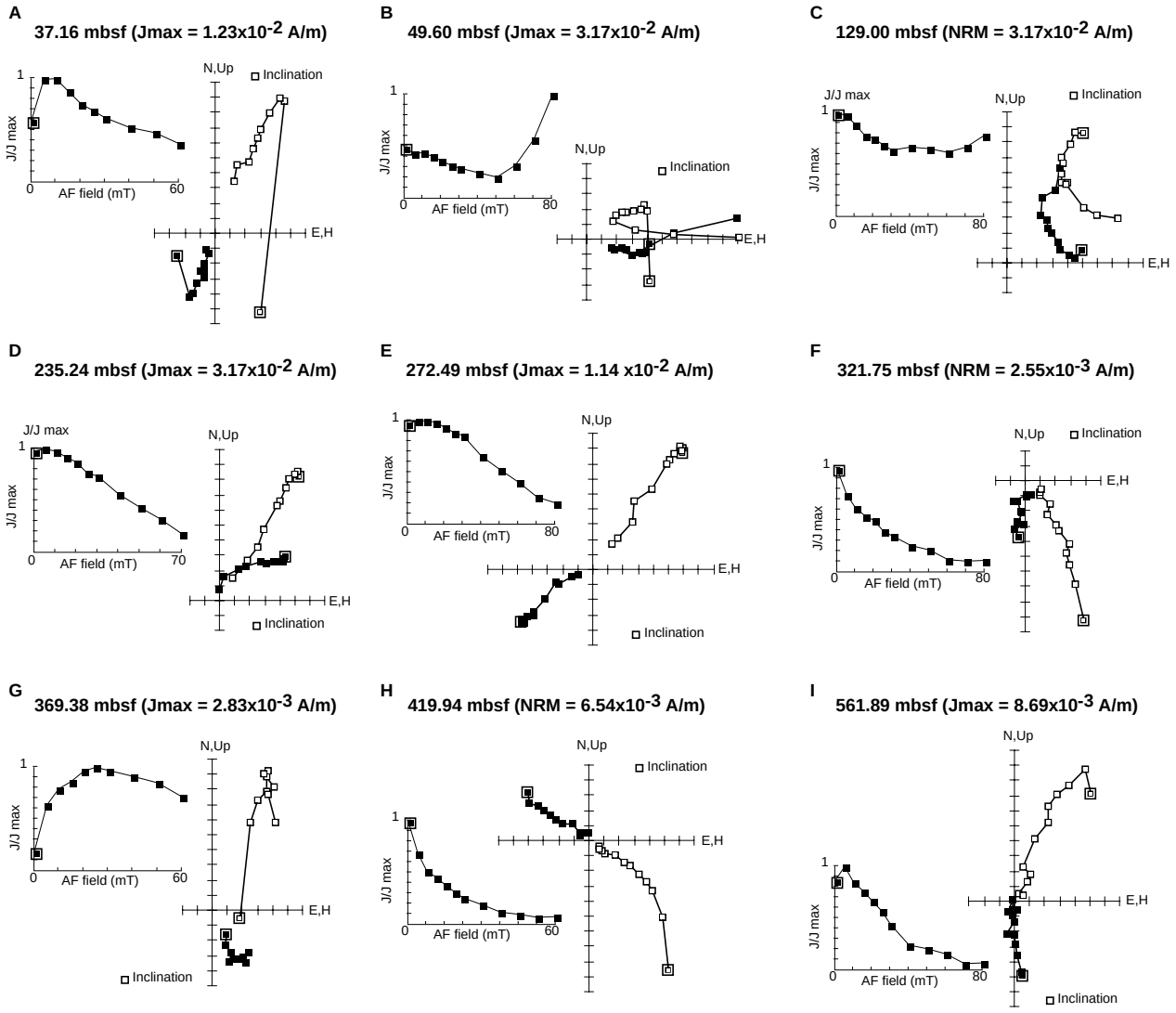

Figure F23. Isothermal remanent magnetization (IRM) and backfield acquisition curves for representative discrete samples from Hole 1122C. **A.** Samples from above 250 mbsf, remanence saturates by 300 mT, and B_{cr} is between 50 and 75 mT. **B.** Samples from 300–400 mbsf, remanence saturates by 300 mT, and B_{cr} is <50 mT. **C.** Samples from beneath 400 mbsf, remanence does not saturate until nearly 1000 mT for samples from 483 and 457 mbsf, B_{cr} values vary between 25 and 75 mT. Remanence does not become saturated until 200–500 mT and B_{cr} is <50 mT for all samples.

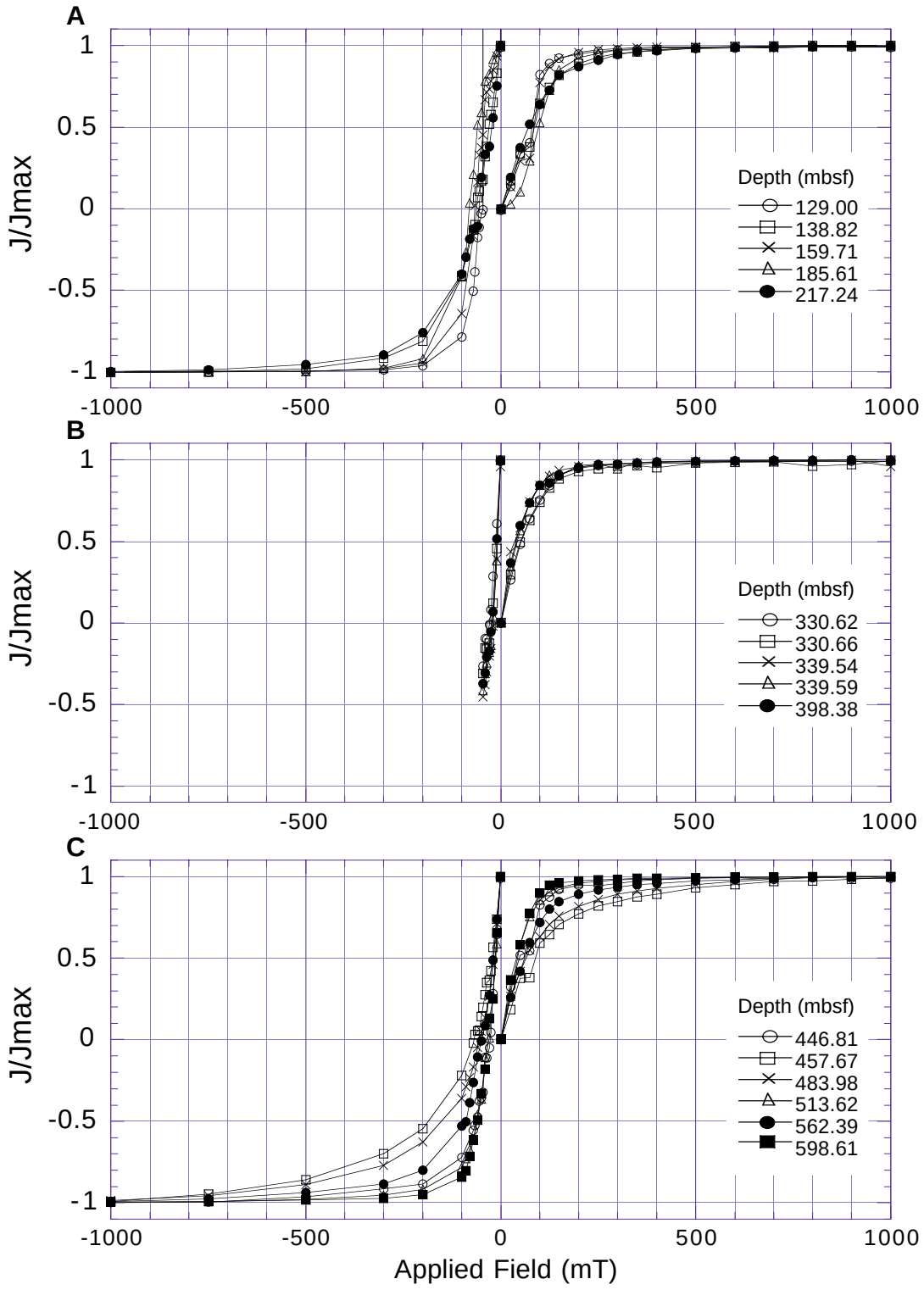

Figure F24. A-F. Plots of normalized intensity of magnetization with progressive AF and thermal demagnetization of saturation isothermal remanent magnetization (SIRM) for selected samples from Hole 1122C.

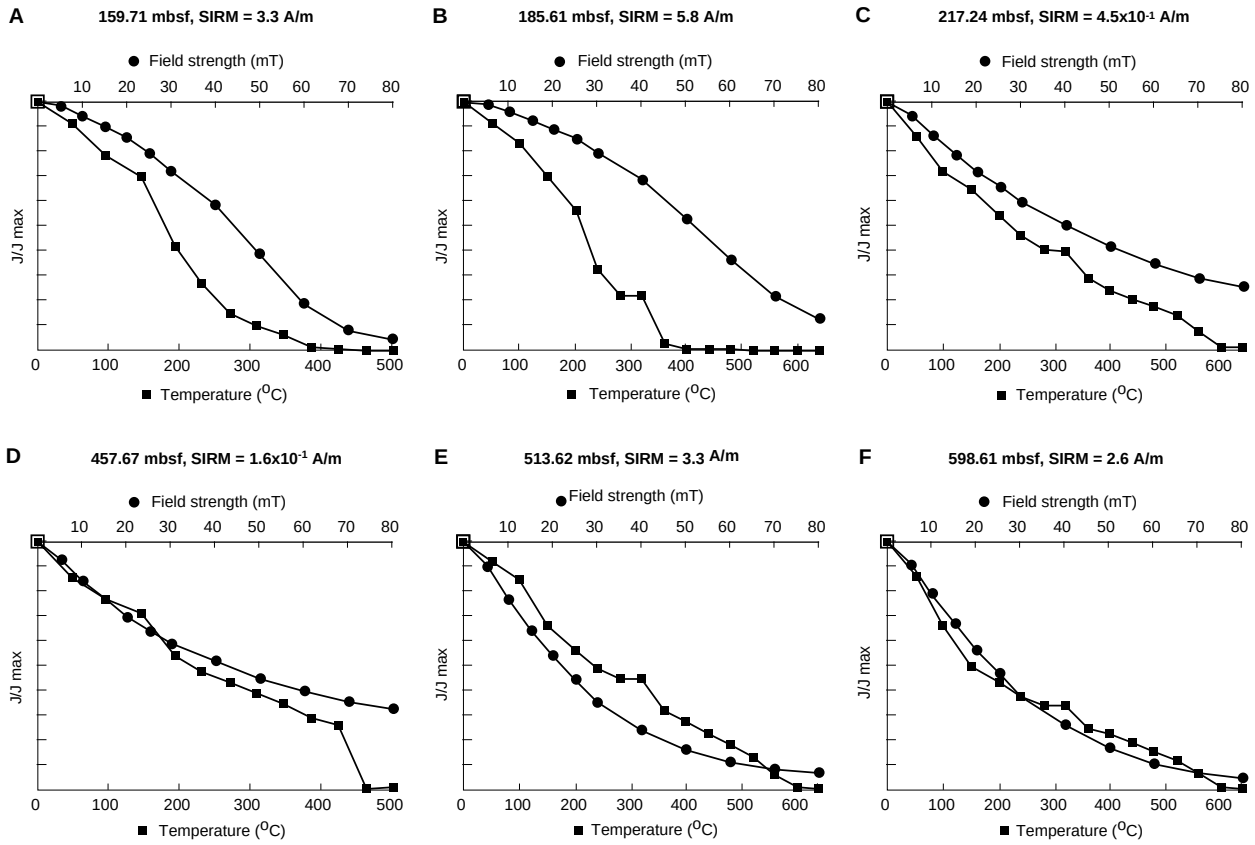

Figure F25. Age model and correlation of Hole 1122C magnetic polarity zonation with the Geomagnetic Polarity Time Scale of Berggren et al. (1995) and Cande and Kent (1995). Where correlation is unambiguous, it is shown by a solid black line. Black (white) shaded intervals indicate normal (reversed) polarity and hatched shading indicates intervals where polarity could not be determined because of nonrecovery. Stippled lines show constraining biostratigraphic datums and shaded lines show magnetic polarity correlations. Undulating lines indicate stratigraphic disconformities and shaded areas indicate levels of uncertainty in datums. Correlation is constrained by the following foraminifer, nannofossil, diatom, and radiolarian datums (see discussion in **"Biostratigraphy,"** p. 13; see also **"Biostratigraphy,"** p. 10, in the "Explanatory Notes" chapter). Foraminifers: F1 (FO of *Gr. hirsuta,* 0.45 Ma), F2 (LO of *Gr. puncticuloides,* 0.7–0.8 Ma), F3 (several forms younger than ~3.4 Ma, see **"Biostratigraphy,"** p. 13), F4 (occurrence of *N. continuosa* and *N. pachyderma,* ~11.3 Ma), F5 (LO of *Gr. praemenardii,* ~13.0 Ma), F6 (co-occurrence of *Gr. zealandica* and *Gr. miozea,* 16.3–16.7 Ma). Nannofossils: N1 (FO of *Emiliania huxleyi,* 0.24 Ma), N2 (LO of *Pseudoemiliania lacunosa,* 0.42 Ma), N3 (LO of *R. asanoi,* 0.83 Ma), N4 (FO of *G. parallela,* 0.9 Ma), N5 (FO of *R. asanoi,* 1.06 Ma), N6 and N7 (range of *Gephyrocapsa* [large], 1.1–1.36 m.y.), N8 (FO of *Gephyrocapsa* [medium], 1.66 Ma), N9 (several forms co-occurring, ~3.45 Ma, see **"Biostratigraphy,"** p. 13), N10 (LO of *C. miopelagicus,* > 10.4 Ma), N11 (FO of *C. macintyrei,* 12.34 Ma), N12 (LO of *S. heteromorphus,* 13.52 Ma), N13 (absence of *C. premacintyrei* FO, <17.4 Ma). Diatoms: D1 (LO of *Hemidiscus karstenii,* 0.18–0.19 Ma), D2 (*H. karstenii,* acme, 0.92 Ma), D3 (LO of *A ingens,* 0.64 Ma), D4 (LO of *T. elliptipora,* 0.65–0.7 Ma), D5 (LO of *Nitzschia denticuloides,* 11.3–22.7 Ma), D6 (LO of *D. dimorpha,* 12.2 Ma), D7 (FO of *S. barboi,* 12.5 Ma). Radiolarians: R1 (LO of *Stylatractus universus,* 0.46 Ma), R2 (LO of *L. nautiloides,* 1.93 Ma), R3 (FO of *E. calvertense,* 1.92 Ma). (**Figure shown on next page.**)

Figure F25 (continued).

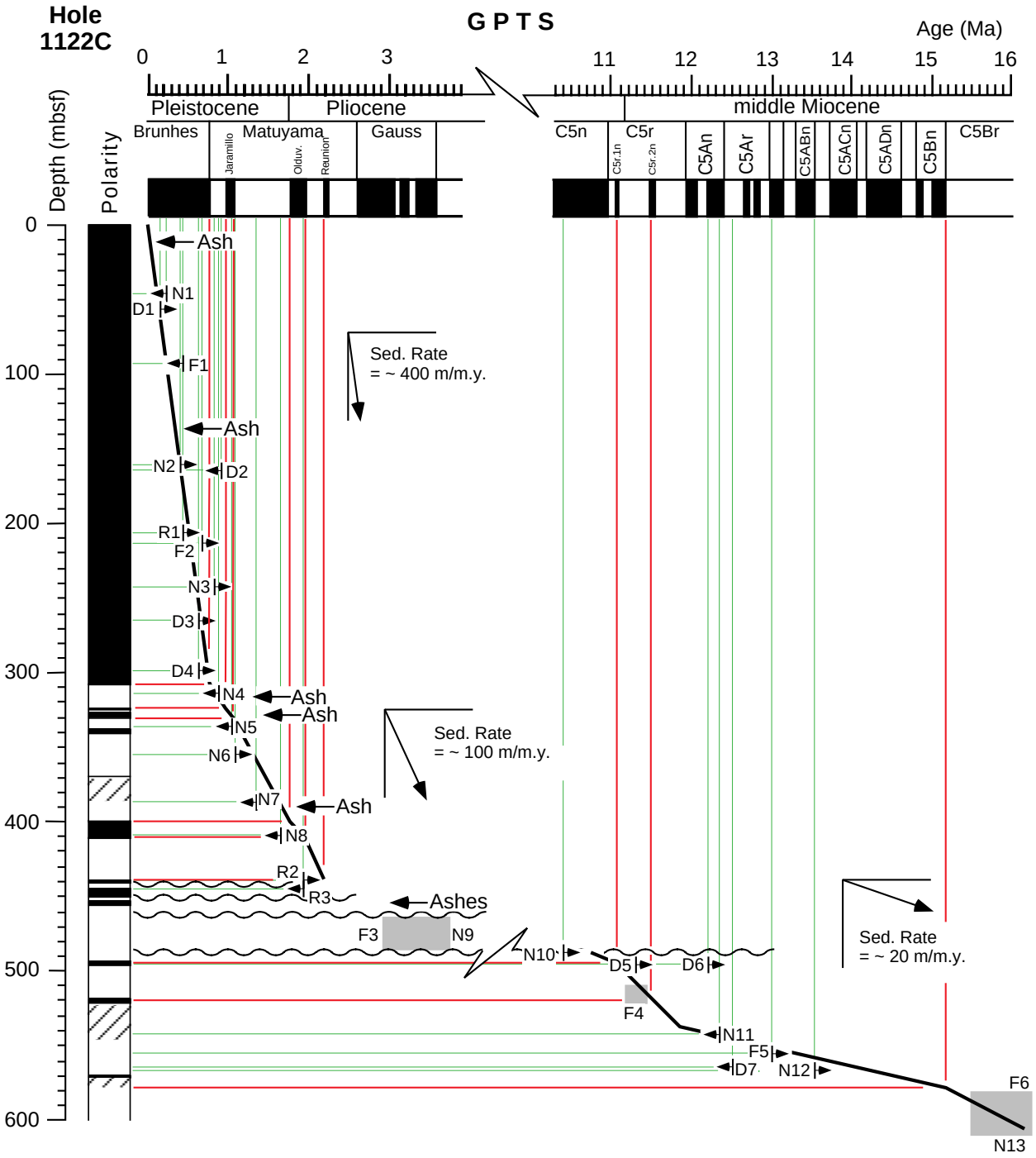

Figure F26. Composite sections for MS, GRAPE, and reflectance percentage at 550 nm. For convenience, MS values from Holes 1122B, 1122C, and Core 181-1122C-3H are offset by 70 × 10^{-5}, 140 × 10^{-5}, and 240 × 10^{-5}, respectively; GRAPE values are offset by 0.4, 0.8, and 1.2 g/cm^3, respectively; and reflectance values are offset by 8%, 16%, and 22%, respectively. Gaps in the composite section are indicated with triangles. Cores are indicated by small numbers. KK indicates the approximate depth of the Kawakawa Tephra (12.62 mcd in Core 181-1122A-1H, 13.14 mcd in Core 2H, and 12.74 mcd in Core 3H). (Continued on next page.)

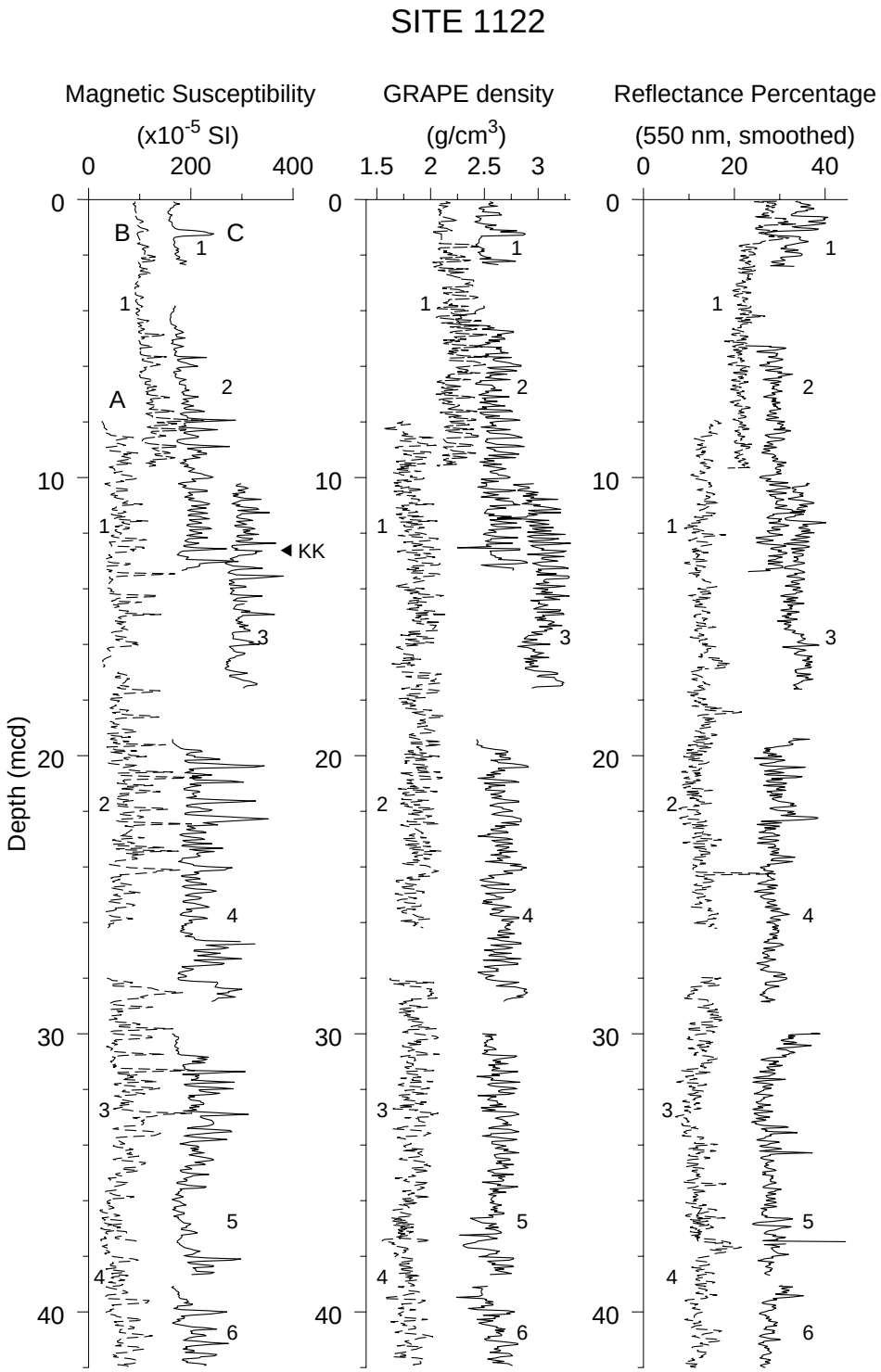

Figure F26 (continued).

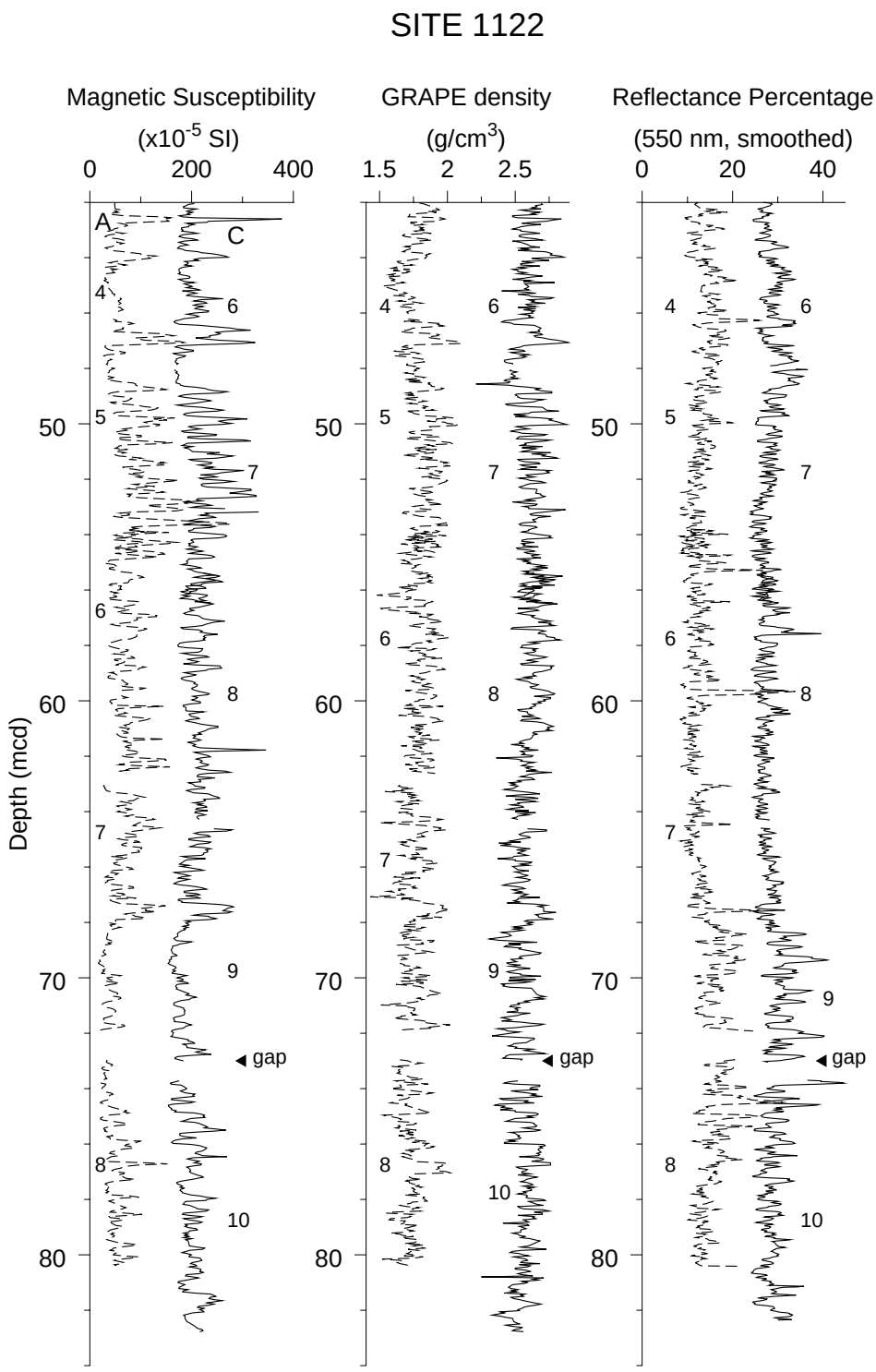

Figure F27. Downhole depth offsets between the mbsf and mcd scales for Site 1122. Solid line indicates the trend for a typical 10% stretch model between mbsf and mcd depths. Composite depth offsets are unusually constant downhole and do not follow a stretch model.